The ATPase Activity of the ChlI Subunit of Magnesium Chelatase and Formation of a Heptameric AAA$^+$ Ring†

James D. Reid, C. Alistair Siebert, Per A. Bullough, and C. Neil Hunter*

Krebs Institute for Biomolecular Research, Department of Molecular Biology and Biotechnology, University of Sheffield, Firth Court, Western Bank, Sheffield S10 2TN, United Kingdom

Received January 15, 2003; Revised Manuscript Received March 21, 2003

ABSTRACT: The AAA$^+$ ATPase component of magnesium chelatase (ChlI) drives the insertion of Mg^{2+} into protoporphyrin IX; this is the first step in chlorophyll biosynthesis. We describe the ATPase activity, nucleotide binding kinetics, and structural organization of the ChlI protein. A consistent reaction scheme arises from our detailed steady state description of the ATPase activity of the ChlI subunit and from transient kinetic analysis of nucleotide binding. We provide the first demonstration of metal ion binding to a specific subunit of any of the multimeric chelatases and characterize binding of Mg^{2+} to the free and $MgATP^{2-}$ bound forms of ChlI. Transient kinetic studies with the fluorescent substrate analogue TNP−ATP show that there are two forms of monomeric enzyme, which have distinct magnesium binding properties. Additionally, we describe the self-association properties of the subunit and provide a structural analysis of the multimeric ring formed by this enzyme in the presence of nucleotide. This single particle analysis demonstrates that this species has a 7-fold rotational symmetry, which is in marked contrast to most members of the AAA$^+$ family that tend to form hexamers.

Magnesium protoporphyrin IX chelatase catalyzes the insertion of a Mg^{2+} ion into protoporphyrin IX. This reaction is the first committed step of (bacterio)chlorophyll synthesis, and it is also one component of a branchpoint in tetrapyrrole biosynthesis, where in the alternative branch ferrous iron is inserted into protoporphyrin leading to the formation of haem. The mechanism of metal ion selection at this branchpoint is crucial as the redox and light-absorbing properties of these tetrapyrroles arise, in part, from the metal ion present, and the resulting haem and chlorophyll cofactors play a central role in energy-transducing complexes.

The magnesium chelatase from the cyanobacterium *Synechocystis* PCC6803 (ChlH, I, D) has been reconstituted in a highly active state following purification of the constituent proteins (*1*, *2*). It consists of three subunits, I (38−42 kDa), D (60−74 kDa), and H (140−150 kDa), in (bacterio)chlorophyll *a* producing prokaryotes (*1*−*3*) and also in higher plants (*4*−*7*).

One generally useful approach to dissect the individual components of magnesium chelatase activity is to examine the reactions of individual subunits. This strategy has led to an overview of the functional role of each subunit and to a quantitative picture of porphyrin binding by the H subunit (*8*). It is widely recognized that the I subunit is an ATPase (*9*−*12*), and it is this activity that drives ion insertion. Little is known, however, about the characteristic behavior of this component, a prerequisite for understanding how this ATPase activity is coupled to the chelation step and is modulated by the different subunits and the other substrates. A high-resolution structure is available for this subunit from *Rhodobacter capsulatus* (BchI), and this work also presents individual EM images of BchI aggregates (*13*). We have performed a single particle structural analysis of the aggregated I subunit using electron microscopy, building upon previous analytical gel filtration studies (*11*, *14*), which clearly showed that ChlI does aggregate in the presence of $MgATP^{2-}$.

Intriguingly, sequence analysis (*15*) of the I and the D subunits and conservation of the characteristic fold in BchI (*13*) show that both of these subunits are members of the AAA$^+$ [1] ATPase family, a group of multimeric enzymes that has a diverse set of cellular roles. The extensive range of activities exhibited by the AAA$^+$ family, which includes DNA replication, membrane fusion, microtubule processing, and proteolysis, appears to be coupled to conformational change, often in a multidomain protein ring, which induces the required change in the macromolecular substrate (*16*, *17*). This could imply that as a small molecule biosynthetic enzyme magnesium chelatase is a rather unusual member of the AAA$^+$ family. However, magnesium chelatase can be viewed as a bifunctional enzyme with an AAA$^+$ ATPase component, which does have a macromolecular substrate, the porphyrin handling H subunit. Spectroscopic studies of the H−porphyrin complex have shown that a conformational change in the porphyrin is likely to be a prerequisite for Mg^{2+} insertion (*8*).

To extend our understanding of the role of the AAA$^+$ ATPase component in the magnesium chelatase reaction, we

† This work was supported by the BBSRC (U.K.).

* To whom correspondence should be addressed. Tel: +44 114 222 4240. Fax: +44 114 222 2711. E-mail: c.n.hunter@sheffield.ac.uk.

[1] Abbreviations: AAA$^+$, ATPases associated with various cellular activities; PNPase, purine nucleotide phosphorylase; v_{ss}, steady state rate; TNP-ATP, 2′,3′-O-(2,4,6-trinitrophenyl)ATP; k_{obs}, observed pseudo-first-order rate constant; *I*, ionic strength.

10.1021/bi034082q CCC: $25.00
Published on Web 05/14/2003

have investigated the structure, nucleotide binding kinetics, and ATPase activity of the ChlI subunit of magnesium chelatase. In particular, the present work integrates (i) a detailed steady state description of the catalytic, ATPase, properties of the ChlI subunit, (ii) a transient state analysis of nucleotide binding, (iii) a detailed study of the self-association properties of the subunit, and (iv) a structural analysis of the multimeric ring formed by this enzyme in the presence of nucleotide.

MATERIALS AND METHODS

Purification of ChlI. The expression vector pET9a-ChlI (*10*) was used to produce recombinant protein essentially as described previously (*2*). Protein was purified by anion exchange chromatography on a Q-Sepharose (Pharmacia) column with a gradient from 250 to 600 mM NaCl over five column volumes in 50 mM Tricine/NaOH, 0.3 M glycerol, 1 mM dithiothreitol (DTT), pH 7.9 (buffer A). The resulting material, which is more than 95% ChlI by sodium dodecyl sulfate polyacrylamide gel electrophoresis (SDS/PAGE), was concentrated to ca. 5 mL, and monomeric ChlI was purified in buffer A, with 200 mM NaCl, by gel filtration on a Sephacryl S-200 HiPrep 26/60 column (Pharmacia) at 0.5 mL/min. Pure protein was flash frozen in and stored under liquid nitrogen. Purification of complexes prior to electron microscopy was carried out by S200 gel filtration as above except that buffer A contained 3 mM ATP, 13 mM $MgCl_2$, and 200 mM NaCl. Nucleotide free protein had a λ_{max} of 280 nm, and protein concentration was determined using the calculated ϵ_{280} of 11 290 M^{-1} cm^{-1} (*18*).

ATPase Assays. The ATPase activity of the ChlI subunit (1 μM) was measured using the EnzChek Phosphate Assay Kit (Molecular Probes Europe BV, Leiden, The Netherlands) essentially as described previously (*10*). Briefly, the chelatase components were incubated with 200 μM 2-amino-6-mercapto-7-methylpurine riboside (MESG) and 1 unit of purine nucleoside phosphorylase (PNPase) in an assay volume of 1 mL. Phosphate release was then measured continuously as an increase in absorbance at 360 nm using a Shimadzu UV2101PC spectrophotometer with a temperature-controlled cuvette holder set at 34 °C. Adventitious phosphate was removed from reaction mixtures by preincubation of the reaction mixture in the absence of added ATPase for 5 min (generally $\Delta A_{360} \cong 0$ after 2 min); this procedure also resulted in thermal equilibration. Reactions were started by the addition of a small volume (typically $\leq$10 μL) of enzyme, and identical traces were seen when the reaction was initiated with $MgCl_2$ and ATP (data not shown). Reactions were carried out at pH 7.7 in 50 mM MOPS−KOH, 0.3 M glycerol, 1 mM DTT at fixed ionic strength, $I = 0.1$, adjusted with KCl and at concentrations of $MgATP^{2-}$ and Mg^{2+} as described in the figure legends. The pH of the reactions did not change during the 5 min assay period or the 5 min preincubation period.

Metal Ion Control. When studying the properties of ATPases, it is important to control the cation/nucleotide equilibrium as a metal bound nucleotide is generally the substrate (*19*). As the free species (e.g., ATP^{4-}, Mg^{2+}) often act as activators or inhibitors, it is useful to investigate the effects of varying their concentration (*19*); this is particularly important in an enzyme that processes magnesium ions. In our reaction mixtures, essentially all ATP is maintained in the $MgATP^{2-}$ form by keeping at least a 1 mM excess of $MgCl_2$ over ATP. The effectiveness of this procedure can be calculated from the stability constants for $MgATP^{2-}$ and the pK_a of the terminal phosphate of ATP (*20*), and the concentration of free nucleotide in our experiments is always less than 5% of total nucleotide.

Analytical Gel Filtration. Gel filtration was performed on a Waters high-performance liquid chromatograph (HPLC) with fluorescence detection ($\lambda_{ex} = 295$ nm, $\lambda_{em} = 340$ nm) and on a hydrophobic-bonded silica matrix (Biosep-SEC-4000, Phenomenex, U.K.) calibrated using the following M_r markers (Sigma, Poole, U.K.): bovine erythrocyte carbonic anhydrase (29 000), bovine serum albumin (66 000), yeast alcohol dehydrogenase (150 000), sweet potato β-amylase (200 000), horse spleen apoferritin (443 000), bovine thyroglobulin (669 000); the void volume was determined with blue dextran. Samples (10 μL aliquots) were either run in 50 mM tricine/KOH, pH 7.5, 200 mM NaCl, 1 mM DTT, or in the same buffer with 5 mM ATP and 10 mM $MgCl_2$.

Stopped Flow Spectroscopy. Kinetic studies were performed on an Applied Photophysics Pi-star spectrophotometer with a 2 mm light path operating in fluorescence mode. Excitation light from a Xenon source passed through a monochromator set at 418 nm with slits set to provide a 6 nm (entrance) and 10 nm (exit) band-pass, and emitted light was detected at 90° through a 515 nm cutoff filter (OG515, Schott). Traces were collected under the conditions described above for steady state kinetics except that final enzyme concentration was 0.5 μM and [TNP−ATP] $\geq$ 5μM. The enzyme syringe contained all of the buffer, and the nucleotide syringe contained all of the $MgCl_2$ and KCl. Reactions were monitored over 0.5−1 s, around 15 overlaying traces were averaged, and k_{obs} values for the formation of the enzyme−ligand complex were evaluated by fitting the time course to the equation for a single exponential process, $A_t = A_0 e^{-k_{obs}t} + A_\infty$, using the data analysis software supplied with the instrument.

Electron Microscopy and Image Analysis. Three microliters of sample (diluted to ca. 0.5 μM ChlI) was rapidly applied to freshly glow-discharged carbon-coated copper grids. Samples were washed twice in distilled water, blotted, and negatively stained with 0.75% (w/v) uranyl formate. Grids were air-dried and subsequently examined in a Lab_6 equipped Philips CM100 electron microscope. Images were acquired at 26 900× magnification on Kodak SO-163 film. Micrographs were developed in PQ developer for 5 min and digitized with a Zeiss SCAI scanner at a 28 μm sample interval corresponding to 10.4 Å at the specimen level.

Images were selected from the micrographs and extracted using Ximdisp (*21*). Band-pass filtered images were iteratively translationally aligned to a rotational sum. Images were classified using multivariate statistical methods in IMAGIC (*22*), which also provided eigenvectors, reflecting the most significant features of images that allowed ready assessment of the rotational symmetry of the images (*23*).

RESULTS

Steady State ATPase Kinetics of the ChlI Subunit: Magnesium Binding and the Dramatic Changes in Affinity between Free and Substrate-Bound Enzyme. The ChlI subunit

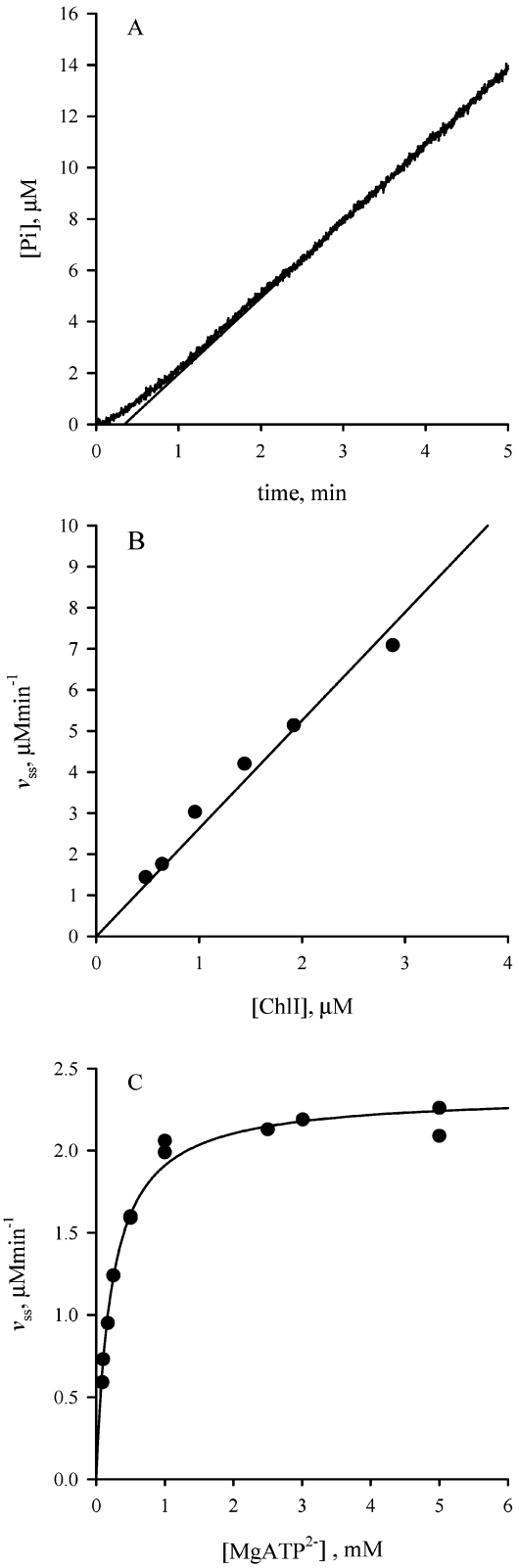

FIGURE 1: ChlI hydrolyses $MgATP^{2-}$ to release phosphate. (A) Release of phosphate during the steady state hydrolysis of $MgATP^{2-}$ by ChlI (1 μM). (B) The steady state rate of phosphate release is linear in [E]. (C) Variation of the steady state rate of $MgATP^{2-}$ hydrolysis with $[MgATP^{2-}]$; at 5mM $[Mg^{2+}]$, the line is described by the Michelis−Menten equation with characterizing parameters of $V = 2.3 \pm 0.04$ μM min^{-1} and $K = 230 \pm 20$ μM.

catalyzes the hydrolysis of $MgATP^{2-}$ (Figure 1). Phosphate release, after a short initial lag phase, can be observed (Figure 1a) using a coupled enzyme assay (*24*). As the rate of phosphate production after the lag is linearly dependent on enzyme concentration (Figure 1b) and as less than 1−2% of substrate has been converted to product, we conclude that steady state rates are being measured. The length of this lag phase is not affected by the concentration of the coupling enzyme (PNPase), the concentration of ChlI used to start the reaction, or the incubation of ChlI with either free nucleotide or $MgCl_2$ before starting the reaction (data not shown). The dependence of the steady state rate (v_{ss}) on $[MgATP^{2-}]$ is hyperbolic (Figure 1c) and so shows no evidence for interaction between ATPase sites or of heterogeneity in these sites. As it is known that low salt concentrations can promote self-association of other AAA^+ family members (*25*, *26*), all reactions were carried out at a constant I of 0.1.

We investigated the role of free magnesium in the ChlI-catalyzed hydrolysis of $MgATP^{2-}$ and demonstrated that it acts as an activator (Figure 2); it has previously been shown that ChlI does not hydrolyze ATP without an excess of $MgCl_2$ over ATP (*10*). When $MgCl_2$ is maintained in a constant excess of nucleotide, the concentration of $MgATP^{2-}$ and ATP^{4-} remains in constant proportion as $[ATP]_T$ is varied. The kinetic consequences of this experimental design, should ATP^{4-} be an inhibitor, have been discussed in detail elsewhere (*19*). This possibility must be considered as ATP^{4-} will always be present in our assay mixtures and will vary in proportion to free magnesium. The predicted dependencies of V and V/K on $MgATP^{2-}$ when ATP^{4-} acts as a competitive inhibitor are that V shows a hyperbolic response and V/K is constant as $[MgCl_2]$ is varied (*19*). This is not observed. The predicted behavior of v_{ss} as a consequence of uncompetitive inhibition by ATP^{4-}, apparent substrate inhibition, is also not seen. We can therefore conclude that ATP^{4-} is not a significant inhibitory species in these experiments and that the observed activation is in fact due to ChlI binding Mg^{2+}.

Further analysis in terms of the activator model (Scheme 1) is particularly simple if substrate and activator binding can be treated as being in quasi-equilibrium, as then effects on V/K reflect activator binding to free enzyme and effects on V reflect binding to enzyme−substrate complexes. There is a significant difference in the effect of magnesium on the observed kinetic parameters V and V/K. Apparent V responds to free magnesium in a hyperbolic fashion with a fairly tight binding, and the response can be described by eq 1a where the maximum rate of the magnesium-bound enzyme, V_{EMg}, is 2.86 ± 0.17 μM min^{-1}, and the binding constant describing the interaction between substrate-bound enzyme and magnesium ions, K_{Mg}', is 1.12 ± 0.29 mM. Unless one step is rate determining, then this binding constant is likely to reflect magnesium binding to a number of discrete species along the reaction pathway.

$$V = \frac{V_{E.Mg}}{1 + \frac{K_{Mg}'}{[Mg^{2+}]}} \text{ (a)}; \frac{V}{K} = \frac{V_{E.Mg}/K_s'}{1 + \frac{K_{Mg}}{[Mg^{2+}]}} \text{ (b)} \qquad (1)$$

The apparent V/K of the ChlI-catalyzed hydrolysis of $MgATP^{2-}$ is also affected by the concentration of free Mg^{2+} except that in this case, a linear relationship is observed. When Mg^{2+} binds to the free enzyme, the hyperbolic relationship between V/K and free Mg^{2+} shown in eq 1b

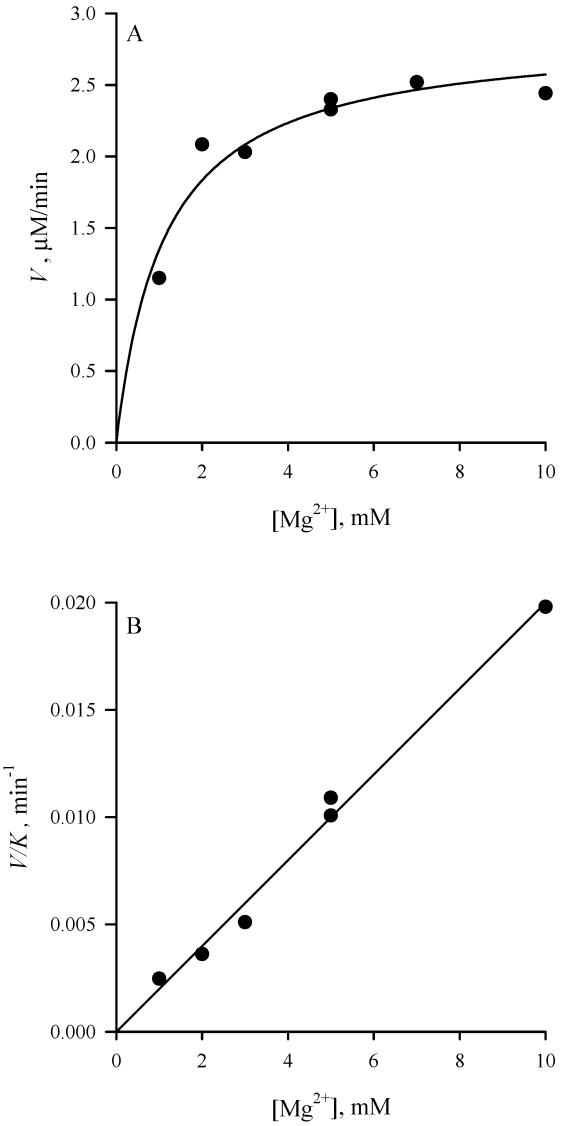

FIGURE 2: Free magnesium ions activate the ChlI-catalyzed hydrolysis of MgATP^{2-}. (A) Variation of apparent V with the concentration of free Mg^{2+} ions. The continuous line is described by eq 1 with characterizing parameters $V_{E.Mg} = 2.86 \pm 0.17$ μM min^{-1} and $K_{Mg}' = 1.12 \pm 0.29$ mM. (B) Variation of apparent V/K for the ChlI-catalyzed hydrolysis of MgATP^{2-} with the concentration of free Mg^{2+}. The points are experimental, and the slope of the straight line, $V_{E.Mg}/K_s'K_{Mg}$, is 0.033 M^{-1} s^{-1}.

Scheme 1: Alternative Pathways for the Binding of Metal Ion and Hydrolysis of MgATP^{2-} Catalyzed by the ChlI Protein[a]

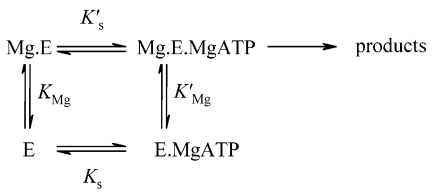

[a] The magnesium dependence of the steady state kinetic parameters is described by eq 1 when activator and substrate binding are in quasi-equilibrium.

would be expected. However, the linear form is observed when $[Mg^{2+}] \ll K_{Mg}$, where K_{Mg} is the dissociation constant of the Mg.E species. These data (Figure 2b) demonstrate that magnesium binding to the free enzyme is relatively weak with a $K_{Mg} \gg 10$mM. This is in sharp contrast to the binding constant between Mg^{2+} and the substrate-bound enzyme, K_{Mg}', of 1.12 mM.

The slope of the straight line in Figure 2b, $V_{E.Mg}/K'_sK_{Mg}$, is 0.033 M^{-1} s^{-1}. We can now calculate the Michaelis constants for MgATP^{2-}; K_s is 1.29 mM and $K_s' \ll 140$ μM (Scheme 1). It is clear that the binding of one ligand greatly affects the binding constant for the other. The free energy associated with this change in binding constants $\Delta\Delta G \ll -5.6$ kJ mol^{-1}, and the consequent increase in affinity of the second site results in very little enzyme bound to a single species, with most of the enzyme present as E or as Mg.E.MgATP^{2-} (Scheme 1).

These results show that Mg^{2+} is an activator for the catalyzed hydrolysis of MgATP^{2-} and that in the steady state the predominant species are (i) free enzyme bound to neither species or (ii) enzyme bound to both Mg−nucleotide and to Mg^{2+}. Our steady state experiments do not allow us to determine the order of formation of these two species but demonstrate that the affinity of the magnesium binding site changes dramatically between free (E) and substrate-bound enzyme (E.MgATP). The magnesium binding constants, K_{Mg} and K_{Mg}', are composite constants that may reflect binding to multiple enzyme forms. The magnesium dependence of individual reaction rate constants determined by transient kinetics will be required to resolve magnesium binding to individual enzyme conformers.

Changes in Mg^{2+} Affinity of the Free Enzyme: Transient Kinetics of TNP−ATP Binding by ChlI. To investigate the binding of magnesium to discrete enzyme forms, we undertook a preliminary transient kinetic study using a fluorescent nucleotide analogue. This provides a convenient probe of nucleotide binding and of any subsequent conformational changes. The analogue TNP−ATP on binding undergoes a shift in λ_{max} from 408 to 418 nm and an enhancement in fluorescence. This nucleotide may allow resolution of magnesium binding to individual conformers on the reaction pathway.

Our data (Figure 3a) show that there is a monoexponential rise in fluorescence on binding of nucleotide and that a large (ca. 60%) proportion of the total fluorescence change occurs within the dead time of the instrument (ca. 1 ms). The k_{obs} value shows an unusual concentration dependence where k_{obs} decreases as the concentration of nucleotide is increased, as seen in the individual curves in Figure 3b. These curves can be described by eq 2. This behavior is characteristic of a two-step mechanism where there is an isomerization of free enzyme and ligand binding is fast, e.g., the lower horizontal pathway in Scheme 2. The increase in signal that occurs within the dead time is primarily due to the rapid binding reaction of the E form. As we observe a marked change in the binding kinetics when $[Mg^{2+}]$ is varied, we extend our scheme to include magnesium binding to all enzyme forms (Scheme 2).

$$k_{obs} = \frac{k_{-1}^{app} K_{ES}^{app}}{K_{ES}^{app} + [S]} + k_{+1}^{app} \quad (2)$$

As a consequence of the spectral characteristics of our system, we are unable to collect pseudo-first-order kinetic data below a [TNP−ATP] of 5 μM. Therefore, K_{ES}^{app} and the

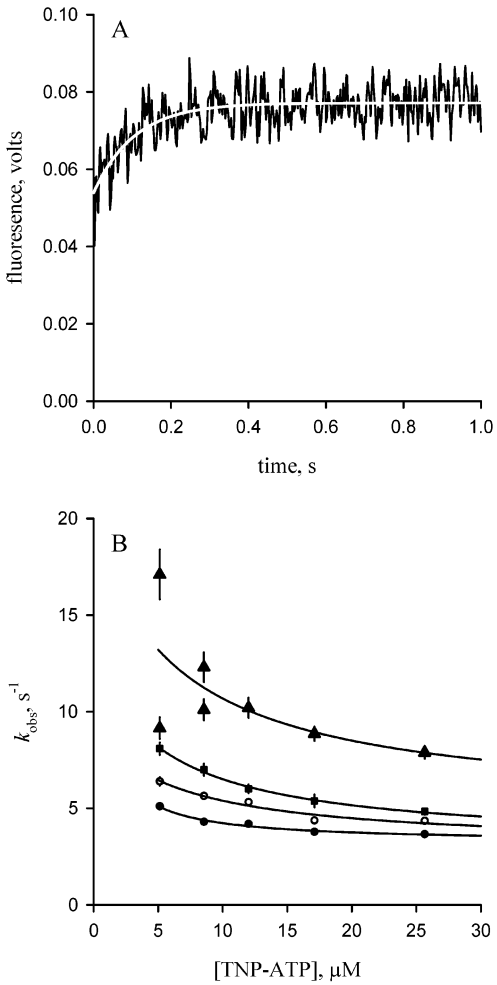

FIGURE 3: Fluorescent nucleotide analogue reveals an isomerization of free ChlI. Dependence on nucleotide concentration of the k_{obs} for the binding of TNP−ATP to ChlI. (A) Average of 15 individual traces with 2 mM $MgCl_2$ and 7.5 μM TNP−ATP; the smooth line is the fitted monoexponential with a $k_{obs} = 9.46 \pm 1.0$ s^{-1}. The trace has had the baseline fluorescence of 7.5 μM TNP−ATP subtracted. (B) A series of profiles showing the k_{obs} values for the binding of TNP−ATP to ChlI at 10 (●), 5 (○), 2.5 (■), and 1 mM (▲) $MgCl_2$. The smooth lines are described by eq 2 with characterizing parameters: 10 mM $MgCl_2$, $k_{+1}^{app} = 3.2 \pm 0.3$ s^{-1}, $k_{-1}^{app} = 16.9 \pm 51.5$ s^{-1}, $K_{ES}^{app} = 0.62 \pm 2.53$ μM; 5 mM $MgCl_2$, $k_{+1}^{app} = 3.0 \pm 1.1$ s^{-1}, $k_{-1}^{app} = 6.2 \pm 2.5$ s^{-1}, $K_{ES}^{app} = 6.2 \pm 8.8$ μM; 2.5 mM $MgCl_2$, $k_{+1}^{app} = 3.1 \pm 0.5$ s^{-1}, $k_{-1}^{app} = 10.0 \pm 1.6$ s^{-1}, $K_{ES}^{app} = 5.2 \pm 2.53$ μM; 1 mM $MgCl_2$, $k_{+1}^{app} = 4.9 \pm 11.4$ s^{-1}, $k_{-1}^{app} = 14.8 \pm 21.5$ s^{-1}, $K_{ES}^{app} = 6.4 \pm 34.5$ μM.

Scheme 2: Binding of Substrate, S, and Activating Metal Ion to Enzyme When the Free Enzyme Isomerizes[a]

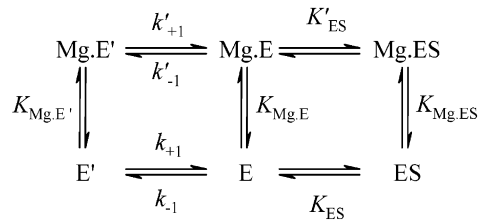

[a] Steps with equilibrium constants (K) are taken as equilibrating much faster than steps shown with a pair of rate constants (e.g., k_{+1}, k_{-1}).

intercept on the k_{obs} axis (i.e., $k_{-1}^{app} + k_{+1}^{app}$) are poorly defined by our data, and while they appear to be magnesium-dependent, it is not appropriate to attempt to quantitatively

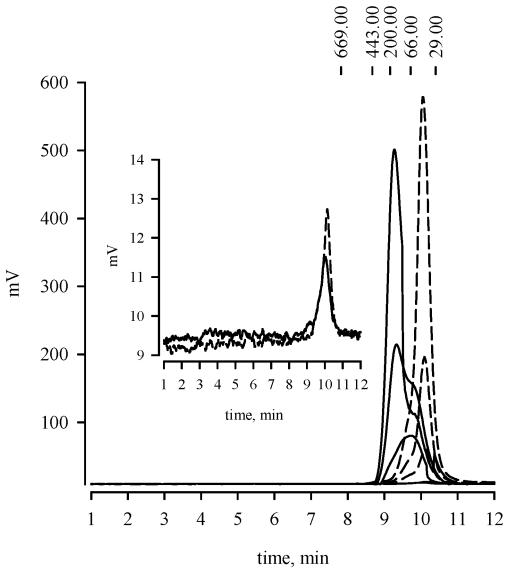

FIGURE 4: Assembly of multimeric ChlI requires substrates and is modulated by protein concentration. From top to bottom, traces are ChlI applied at 56, 28, 11, and 1.1 μM (inset) with the late eluting peaks (ca. 10 min, dotted lines) without added nucleotide and the early eluting peaks (ca. 9−10 min, solid lines) in the presence of 10 mM $MgCl_2$ and 5 mM ATP. The elution position of the standards is shown above the traces with their relative molecular masses. The inset shows the elution of 1.1 μM ChlI under both conditions.

explain their behavior. The overall trend is clear however and allows assignment of this reaction to the mechanism shown above (Scheme 2). The family of curves (Figure 3b) obtained as the magnesium concentration was varied converges at high nucleotide concentration, which suggests that k_{+1}^{app} is not affected by free magnesium and so reflects k_{+1} in Scheme 2. The data in Figure 3b lead to the conclusion that the I subunit undergoes a slow isomerization and that this process is affected by Mg^{2+}. The K_d for TNP−ATP obtained in static binding experiments is in the micromolar range (3.7 μM at 2 mM Mg^{2+}, data not shown) and millimolar ATP is required to displace this analogue (data not shown) suggesting that TNP−ATP and ATP compete for a binding site.

Oligomerization of ChlI Is Mediated by Protein Concentration and by Magnesium−Nucleotide Complex. Analytical gel filtration was used to investigate the self-association behavior of ChlI. Varying concentrations of ChlI (1.1−56 μM) were applied to a gel filtration column either with or without added nucleotide and metal ion (5 mM ATP, 10 mM $MgCl_2$). When the nucleotide and metal ion were present, they were in both the running buffer and the protein sample. Chromatograms (Figure 4) were obtained from protein fluorescence using excitation at 295 nm ($\lambda_{em} = 340$ nm) to avoid the significant interfering nucleotide absorbance. The protein used in this series of experiments had been purified as a monomer by preparative scale gel filtration and, as indicated by the absorbance spectra (data not shown), contained no contaminating nucleotides.

When no nucleotide or magnesium is present, it can be seen that ChlI elutes with one well-defined peak at 10.1 min, which corresponds to a monomer. These elution profiles also contain a minor component eluting at around 9.8 min, which may reflect dimer or trimer formation. In contrast, when substrates are present and at high ChlI concentration, the

main elution peak is at 9.3 min. Although this apparently corresponds to oligomers composed of 5 or 6 ChlI molecules, we assign this peak to a heptamer on the basis of our single particle analysis (see below). The slight difference in observed and predicted elution position is most probably a consequence of the heptameric complex deviating significantly from the ideal spherical shape. Such deviations have been previously observed in heptameric AAA$^+$ species (*26*). The shoulder on the trailing edge of these peaks is due to the presence of intermediate size fractions. Significantly, at low protein concentrations (1 μM, Figure 4 inset), ChlI elutes at 10.1 min whether $MgATP^{2-}$ is present. This is characteristic of monomer and demonstrates that a high ChlI concentration is required to form the heptameric form of the enzyme even in the presence of substrate. As protein concentration increases, when $MgATP^{2-}$ is present, the relative proportions of the three forms, monomer, intermediate oligomer, and heptamer, change. At more than 25 μM ChlI, the predominant species is heptameric and the monomer is undetectable at more than 10 μM protein.

Single Particle Analysis of the ChlI Complex. Multimeric ChlI was purified by gel filtration in the presence of 10 mM $MgCl_2$ and 5 mM ATP. The elution time was consistent with a high M_r form of ChlI. This material was diluted (to ca. 0.5 μM) and applied directly and rapidly to freshly glow-discharged carbon-coated grids, negatively stained with uranyl formate and examined at 26 900× magnification (Figure 5).

The image analysis methods used have been described elsewhere (*22*, *27*). Raw images were band-pass filtered to remove low and high spatial frequency components and translationally aligned to a rotational average of the entire image set. A preliminary characterization of the entire data set provided a subset of images ($n = 162$) that appear to be projections down an axis of rotational symmetry and are broadly circular. This subset was analyzed further. Translationally aligned images (e.g., Figure 5a) were classified using multivariate statistical procedures. An eigenimage analysis provides evidence of 7-fold rotational symmetry (Figure 5b). Images were grouped into classes, and characteristic class average images were used as references during translational and rotational alignment of the data. This procedure provided a good superimposition of all top views that when averaged (Figure 5c), clearly show 7-fold rotational symmetry. This assignment is further supported by our harmonic analysis (Figure 5d).

DISCUSSION

We have presented here a detailed characterization of the ATP hydrolyzing activity of the ChlI subunit of magnesium chelatase from *Synechocystis* and demonstrated that it is a magnesium binding subunit. We have further characterized the nucleotide and magnesium binding properties of this subunit with transient kinetic studies of the interaction with the fluorescent analogue TNP−ATP and shown that the two distinct forms of enzyme have very different magnesium binding properties. Our analytical gel filtration has clarified the conditions under which the reported (*12*−*14*) high M_r oligomeric form of the magnesium chelatase I subunit is formed, and our single particle analysis has demonstrated that this species has a 7-fold rotational symmetry. Our results are summarized in Scheme 3.

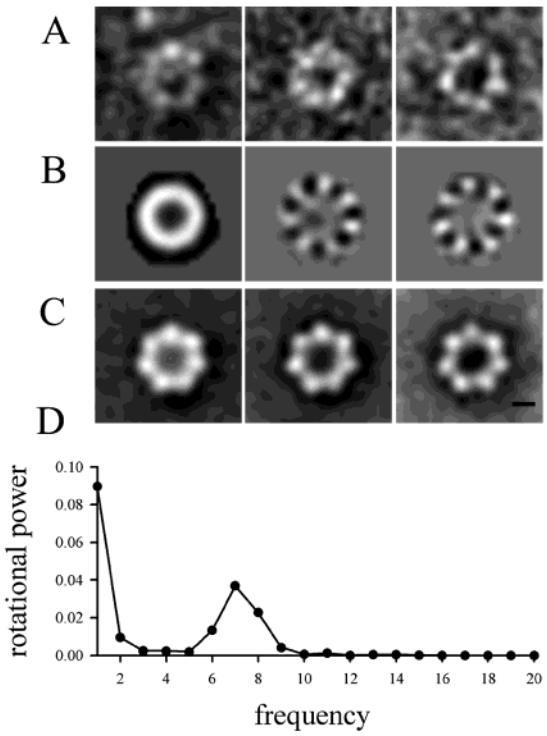

FIGURE 5: Organization of the ChlI subunit into heptameric rings. Symmetry analysis of 162 images of negatively stained ChlI, at a magnification of 26 900×. Scale bar, bottom right, 100 Å. (A) Representative images after application of a Gaussian filter to remove high and low spatial frequency information and reference free translational alignment; (B) the first, third, and fourth eigenimages of the multivariate statistical analysis; (C) class averages; (D) rotational power spectrum for translationally and rotationally aligned ChlI images. The image was floated in a circular box with the radius of the ring. The boxed density was floated into a large square box and analyzed with the program RFILTIM (*29*).

Scheme 3: Integrated View of the Behavior of the ChlI Subunit[a]

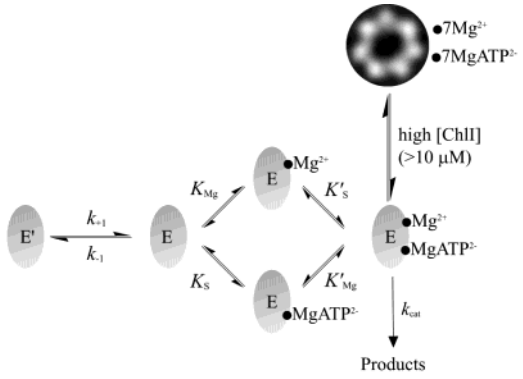

[a] All steps have been investigated kinetically except for the self-assembly of ChlI, which has been examined by a combination of analytical gel filtration and single particle electron microscopy. We estimate the isomerization rate constants k_{+1} as 3.1 s^{-1} and k_{-1} as ca. 10 s^{-1}; the turnover number k_{cat} is 0.05 s^{-1} assuming that the enzyme is 100% active. The ATPase activity of the heptamer has not been characterized. Binding constants $K_{Mg} \gg 10$ mM, $K_{Mg}' = 1.12$ mM, $K_s = 1.29$ mM, and $K_s' \ll 140$ μM.

Magnesium Ions Bind to the ChlI Subunit and Activate Hydrolysis of MgATP^{2-}. It has been previously shown that the magnesium chelatase I subunit of *Synechocystis* PCC6803 (*10*), *Rhodobacter sphaeroides* (*12*), and *Chlorobium vibrioforme* (*9*) will catalyze the hydrolysis of $MgATP^{2-}$. Without characterizing the kinetic parameters *V*, *V*/*K*, and their

dependence on Mg^{2+}, the ATPase efficiencies of various wild-type and mutant chelatases and their component subunits cannot be compared. We have determined the steady state kinetic parameters of the ChlI-catalyzed hydrolysis of $MgATP^{2-}$ at a free Mg^{2+} concentration of 5 mM (Figure 1). Our data can be described by a simple model, which does not provide any evidence for cooperativity or for substrate inhibition. It has been demonstrated, however, that in the presence of $MgATP^{2-}$ both ChlI (*14*) and BchI (*12*, *13*) form multimers. The aggregates of ChlI most probably contain seven subunits (see below). Our analytical gel filtration (Figure 3) shows that ChlI is essentially monomeric under the conditions used in our steady state kinetic experiments. These conclusions can be contrasted with those of a recent report of the ATPase properties of wild-type and mutant *R. capsulatus* BchI subunit (*11*). These authors conclude on the basis of analytical gel filtration that BchI forms aggregates and argue that this species, presumed to be a hexamer by analogy to other AAA^+ family members (*13*), is the active ATPase species in their assays. As their gel filtration of BchI aggregates was carried out with ca. 75 μM BchI and the steady state ATPase assays were performed with 0.2 μM enzyme, we suggest that BchI was either monomeric in the assay or that it has very different self-association properties to ChlI (see Figure 4). This suggestion, that these observed ATPase activities for BchI (*11*) relate to the monomeric species, is consistent with the observation that the ATPase activities of mixtures of wild-type and mutant BchI correspond to the sum of the separately measured activities. However, no conclusion can then be made about the role of these residues in the ATPase activity of aggregated BchI in the absence of other subunits. In contrast, these residues (D207N, R289K, and L111F; *R. capsulatus* numbering) do appear to have a role in the interface between BchI molecules within the intact magnesium chelatase (*11*).

We have shown here that the ChlI subunit of magnesium chelatase binds to free Mg^{2+} as well as catalyzes the hydrolysis of $MgATP^{2-}$ (Figure 2). This is the first demonstration of free magnesium binding to a specific subunit of any of the multimeric chelatases, and this suggests that the role of free metal ions would be worth exploring throughout the AAA^+ superfamily. These results have a particular significance for the mechanism of magnesium chelatase, because in order to link an ATPase cycle to a catalyzed chelation the free energy derived from nucleotide binding and hydrolysis has to drive magnesium insertion, by producing concomitant changes in the magnesium affinity in both the porphyrin and the protein Mg^{2+} binding sites. While our data do not address the situation in the intact chelatase, we have shown that in the case of the isolated I subunit the dissociation constant changes from $\gg$10 mM from the free enzyme to 1.12 mM from the substrate-bound enzyme. This difference corresponds to a $\Delta\Delta G$ of $\ll -5.6$ kJ mol^{-1}. It should be remembered that the disassociation constant for the magnesium ion and the nucleotide-bound enzyme (K_{Mg}') is a function of the affinities of all intermediates along the reaction pathway, so we cannot ascribe this disassociation constant to a particular enzyme-bound intermediate. As the catalytic activity of the intact chelatase has a cooperative response to Mg^{2+} (*14*), it is clear that either additional metal ion binding sites exist or that the properties of the Mg^{2+} binding sites in ChlI are perturbed in the intact enzyme. The full process can only be observed in the intact chelatase with bound porphyrin, but we have demonstrated that the isolated ChlI subunit shows discrete changes in the affinity of a Mg^{2+} binding site during the ATPase cycle and that $MgATP^{2-}$ hydrolysis is only possible when the I subunit binds free magnesium. More subtle changes in magnesium affinity will be revealed by further, more detailed, transient state kinetics.

While it is tempting to assume that ChlI is the prototypical Mg^{2+} delivering unit in the intact chelatase, there may be additional magnesium binding sites in other subunits. For example, such a binding site was proposed for the D subunit on the basis of sequence similarity to the MIDAS motif of integrin I domains (*13*). Magnesium binding sites are not linked to a clearly defined motif but frequently involve carboxylic acid and hydroxyl side chains (*28*); consequently, it is not possible to readily identify such a site in the ChlI sequence or structure, particularly since there is a number of highly conserved suitable residues in ChlI. If magnesium activation is not a common property across the AAA^+ superfamily, then it may be worthwhile to examine insertions in the I sequence not generally found in the other family members. In particular, the three hairpin loops, $\tau 1 - \tau 3$, found in BchI (*13*) and conserved in ChlI, contain a number of candidate residues, which are not present in other AAA^+ family members.

Nucleotide Binding to the ChlI Subunit. As a step toward determining the magnesium affinities of discrete intermediates in the ATP hydrolysis pathway, we investigated the magnesium dependence of the kinetics of binding of the fluorescent nucleotide analogue TNP−ATP. The kinetics of TNP−ATP binding, however, do not reveal processes occurring within enzyme−substrate complexes but instead provide insight into the free enzyme species. The behavior of k_{obs} as [TNP−ATP] is varied is characteristic of a mechanism (Scheme 2) where the second step, binding of nucleotide, is fast as compared to the rate-determining isomerization of free enzyme. Any subsequent changes in conformation after nucleotide binding do not influence the kinetic behavior of this system. There is no observable hydrolysis of this analogue under the conditions used in our stopped flow experiments (data not shown). This particular analogue appears best suited to reporting on the conformational changes of monomeric free ChlI.

Although it is difficult to resolve the systematic changes in TNP−ATP binding kinetics as we vary [Mg^{2+}], it is clear that k_{+1}, the rate constant for formation of nucleotide-bound enzyme, essentially does not change with the concentration of free ion and that the differences in profile shape can be attributed to k_{-1} and K_{ES}. We conclude that the E and ES forms bind magnesium, in contrast to the E′ form of the I subunit where this has not been observed. This is consistent with the steady state data, summarized in Scheme 1, which show magnesium binding to the free enzyme with a $K_{Mg} \gg$ 10 mM. This macroscopic constant could reflect binding to a range of enzyme forms. However, our transient state data have clarified this picture and suggest that E in Scheme 2 is the predominant form of enyzme, which binds magnesium. We therefore conclude that the steady state data reveal the binding characteristics of the E form and that the composite binding constant K_{Mg} in Scheme 1 is equivalent to K_{MgE}, the specific binding constant of the E form of enzyme, in Scheme 2. We conclude that the I subunit undergoes a slow

isomerization and that Mg^{2+} exerts an influence on this process. This isomerization, with rate constants k_{+1} 3.1 s^{-1} and k_{-1} ca. 10 s^{-1}, occurs on a faster time scale than the rate-determining catalytic steps as k_{cat}, the turnover number for the active magnesium-bound enzyme, is 0.05 s^{-1}.

Self-Assembly of ChlI and Single Particle Analysis of the High M_r Complex. Previous gel filtration studies on the ChlI system (*14*) demonstrated the aggregation of ChlI into a high M_r form containing 6−8 subunits in the presence of $MgATP^{2-}$ and Mg^{2+} (2 and 4 mM, respectively). We have demonstrated here that this high M_r complex requires nucleotide substrate and a high protein concentration (Figure 3). It is clear that the monomeric form is capable of hydrolyzing $MgATP^{2-}$ in the absence of protein−protein interactions (Figure 1). This aggregated form has attracted interest as it may provide insight into the molecular organization of the entire magnesium chelatase. For example, the ChlI heptameric ring may act as a scaffold for the other members of the complex. One quite specific structural model (*13*) proposes that the negatively charged helix between the N- and the C-terminal domains of the ChlD subunit binds to a deep positively charged groove on ChlI, a model that suggests a one-to-one stoichometry between ChlI and ChlD. It is possible that the oligomeric form and geometry of the I type subunits (i.e., ChlI or the N-terminal region of ChlD) within the magnesium chelatase complex directly reflect that of the I ring in solution. Structural information on this species is clearly of interest in increasing our understanding of the architecture of the entire complex. This is a natural progression from the previous X-ray crystallography on the monomeric I subunit and unrefined single particle images (*13*). The unrefined data that led to the previous interpretation that BchI adopts a hexameric form are consistent with our conclusions. In particular, the observed particle size is similar but image processing would be required to demonstrate a particular multimeric structure, a point made by the authors (*13*). It is interesting to note that the C-terminal helical domain of BchI adopts a different orientation to the N-terminal domain as compared to other structurally characterized members of this family (*13*); this structural variation may lead to the observed differences in self-association properties between ChlI and some other members of the AAA$^+$ family. Our analysis demonstrates that ChlI forms seven-membered rings with a diameter of ca. 150 Å. It is common for AAA$^+$ family members to form multimeric rings in the presence of nucleotides although these rings most often contain six members (*17*). Heptameric rings are not unknown, however (*26*), and because only a few of the large AAA$^+$ family have been characterized at any level of structural detail, it remains to be established what the relative proportions of the various oligomeric forms are in this family.

CONCLUSIONS

We have characterized the ATPase activity of the ChlI subunit and have demonstrated that free Mg^{2+} is an activator of the catalyzed hydrolysis of $MgATP^{2-}$. This is the first demonstration of magnesium binding to any subunit of magnesium chelatase. An integrated view of the behavior of the ChlI subunit is shown in Scheme 3. The effects of [Mg^{2+}] on the kinetic parameters V and V/K demonstrate that magnesium ions bind much more tightly to the enzyme−magnesium nucleotide complex than to free enzyme. We conclude that as ChlI passes through a reaction cycle it undergoes stepwise changes in Mg^{2+} affinity, potentially a key part of the chelatase reaction cycle. The I subunit only catalyzes the hydrolysis of $MgATP^{2-}$ when an additional Mg^{2+} is bound. Transient kinetic analysis of the binding of the fluorescent ATP analogue TNP−ATP reveals an isomerization of the ChlI subunit and that one isomer of the free enzyme binds magnesium, results that are fully consistent with our steady state rate data. This isomerization is not rate-determining in our steady state reactions.

Gel filtration has been used to characterize the self-association behavior of ChlI, and we have clearly demonstrated that a multimeric aggregate is formed in the presence of Mg^{2+} and $MgATP^{2-}$ and that the extent of aggregation depends on protein concentration. Three distinct oligomeric forms of enzyme are seen as the protein concentration is increased in the presence of Mg^{2+} and $MgATP^{2-}$. Electron micrographs of the high M_r form demonstrate that it is a heptameric ring with a diameter of ca. 150 Å.

As a whole, these data represent a substantial extension of our understanding of the ATPase characteristics of magnesium chelatase and lay the groundwork for detailed investigations of the self-assembly of the intact enzyme. Additionally, these data offer information on an additional example of an AAA$^+$ ATPase suggesting that the role of free magnesium ions could be relevant across the superfamily and that heptameric aggregates could be more common than currently appreciated. As the intact fully functional magnesium chelatase complex is essentially an AAA$^+$ ATPase module attached to an exceptionally sensitive spectroscopic reporter protein containing porphyrin or metalloporphyrin (*8*), we expect that this system will prove to be a generally useful example in further investigations of AAA$^+$ function.

ACKNOWLEDGMENT

We thank Peiyi Wang for assistance with microscopy. The Krebs Institute is a designated BBSRC Biomolecular Science Center and a member of the North of England Structural Biology Centre.

REFERENCES

1. Gibson, L. C. D., Willows, R. D., Kannangara, C. G., von Wettstein, D., and Hunter, C. N. (1995) Magnesium-protoporphyrin chelatase of *Rhodobacter sphaeroides*: reconstitiution of activity by combining the products of the *bchH*, *-I* and *-D* genes expressed in *Escherichia coli*. *Proc. Natl. Acad. Sci. U.S.A. 92*, 1941−1944.
2. Jensen, P. E., Gibson, L. C. D., Henningsen, K. W., and Hunter, C. N. (1996) Expression of the *chlI*, *chlD*, and *chlH* genes from the cyanobacterium *Synechocystis* PCC6803 in *Escherichia coli* and demonstration that the three cognate proteins are required for magnesium-protoporphyrin chelatase activity. *J. Biol. Chem. 271*, 16662−16667.
3. Petersen, B. L., Jensen, P. E., Gibson, L. C. D., Stummann, B. M., Hunter, C. N., and Henningsen, K. W. (1998) Reconstitution of an active magnesium chelatase enzyme complex from the *bchI*, *D* and *H* gene products of the green sulphur bacterium *Chlorobium vibrioforme* expressed in *E. coli*. *J. Bacteriol. 180*, 699−704.
4. Jensen, P. E., Willows, R. D., Petersen, B. L., Vothknecht, U. C., Stummann, B. M., Kannangara, C. G., von Wettstein, D., and Henningsen, K. W. (1996) Structural genes for Mg-chelatase subunits in barley: *Xantha-f*, *-g* and *-h*. *Mol. Gen. Genet. 250*, 383−394.
5. Gibson, L. C. D., Marrison, J. L., Leech, R. M., Jensen, P. E., Bassham, D. C., Gibson, M., and Hunter, C. N. (1996) A putative Mg chelatase subunit from *Arabidopsis thaliana* cv C24. Sequence

and transcript analysis of the gene, import of the protein into chloroplasts, and in situ localization of the transcript and protein. *Plant Physiol. 111*, 61−71.
6. Kannangara, C. G., Vothknecht, U. C., Hansson, M., and von Wettstein, D. (1997) Magnesium chelatase: association with ribosome and mutant complementation studies identify barley subunit Xantha-G as a functional counterpart of *Rhodobacter* subunit *BchD*. *Mol. Gen. Genet. 254*, 85−92.
7. Papenbrock, J., Gräfe, S., Kruse, E., Hänel, F., and Grimm, B. (1997) Mg-chelatase of tobacco: identification of a *Chl D* cDNA sequence encoding a third subunit, analysis of the interaction of the three subunits with the yeast two-hybrid system, and reconstitution of the enzyme activity by coexpression of recombinant CHL D, CHL H and CHL I. *Plant J. 12*, 981−990.
8. Karger, G. A., Reid, J. D., and Hunter, C. N. (2001) Characterization of the binding of deuterioporphyrin IX to the magnesium chelatase H subunit and spectroscopic properties of the complex. *Biochemistry 40*, 9291−9299.
9. Petersen, B. L., Kannangara, C. G., and Henningsen, K. W. (1999) Distribution of ATPase and ATP-to-ADP phosphate exchange activities in magnesium chelatase subunits of Chlorobium vibrioforme and Synechocystis PCC6803. *Arch. Microbiol. 171*, 146−150.
10. Jensen, P. E., Gibson, L. C. D., and Hunter, C. N. (1999) ATPase activity associated with the magnesium-protoporphyrin IX chelatase enzyme of *Synechocystis* sp. PCC6803: evidence for ATP hydrolysis during Mg^{2+} insertion, and the MgATP-dependent interaction of the ChlI and ChlD subunits. *Biochem. J. 339* (Pt. 1), 127−134.
11. Hansson, A., Willows, R. D., Roberts, T. H., and Hansson, M. (2002) Three semidominant barley mutants with single amino acid substitutions in the smallest magnesium chelatase subunit form defective AAA+ hexamers. *Proc. Natl. Acad. Sci U.S.A. 99*, 13944−13949.
12. Gibson, L. C. D., Jensen, P. E., and Hunter, C. N. (1999) Magnesium chelatase from *Rhodobacter sphaeroides*: initial characterization of the enzyme using purified subunits and evidence for a BchI−BchD complex. *Biochem. J. 337* (Pt. 2), 243−251.
13. Fodje, M. N., Hansson, A., Hansson, M., Olsen, J. G., Gough, S., Willows, R. D., and Al Karadaghi, S. (2001) Interplay between an AAA module and an integrin I domain may regulate the function of magnesium chelatase. *J. Mol. Biol. 311*, 111−122.
14. Jensen, P. E., Gibson, L. C. D., and Hunter, C. N. (1998) Determinants of catalytic activity with the use of purified I, D and H subunits of the magnesium protoporphyrin IX chelatase from *Synechocystis* sp. PCC6803. *Biochem. J. 334* (Pt. 2), 335−344.
15. Neuwald, A. F., Aravind, L., Spouge, J. L., and Koonin, E. V. (1999) AAA(+): A class of chaperone-like ATPases associated with the assembly, operation, and disassembly of protein complexes. *Genome Res. 9*, 27−43.
16. Dalal, S., and Hanson, P. I. (2001) Membrane traffic: what drives the AAA motor? *Cell 104*, 5−8.
17. Vale, R. D. (2000) AAA proteins. Lords of the ring. *J. Cell Biol. 150*, F13−F19.
18. Gill, S. C., and von Hippel, P. H. (1989) Calculation of protein extinction coefficients from amino acid sequence data. *Anal. Biochem. 182*, 319−326.
19. Morrison, J. F. (1979) Approaches to kinetic studies on metal-activated enzymes. *Methods Enzymol. 63*, 257−294.
20. O'Sullivan, W. J., and Smithers, G. W. (1979) Stability constants for biologically important metal−ligand complexes. *Methods Enzymol. 63*, 294−336.
21. Crowther, R. A., Henderson, R., and Smith, J. M. (1996) MRC image processing programs. *J. Struct. Biol. 116*, 9−16.
22. van Heel, M., Harauz, G., Orlova, E. V., Schmidt, R., and Schatz, M. (1996) A new generation of the IMAGIC image processing system. *J. Struct. Biol. 116*, 17−24.
23. Dube, P., Tavares, P., Lurz, R., and van Heel, M. (1993) The portal protein of bacteriophage SPP1: a DNA pump with 13-fold symmetry. *EMBO J. 12*, 1303−1309.
24. Webb, M. R. (1992) A continuous spectrophotometric assay for inorganic phosphate and for measuring phosphate release kinetics in biological systems. *Proc. Natl. Acad. Sci. U.S.A. 89*, 4884−4887.
25. Hattendorf, D. A., and Lindquist, S. L. (2002) Cooperative kinetics of both Hsp104 ATPase domains and interdomain communication revealed by AAA sensor-1 mutants. *EMBO J. 21*, 12−21.
26. Kim, K. I., Cheong, G. W., Park, S. C., Ha, J. S., Woo, K. M., Choi, S. J., and Chung, C. H. (2000) Heptameric ring structure of the heat-shock protein ClpB, a protein- activated ATPase in *Escherichia coli*. *J. Mol. Biol. 303*, 655−666.
27. van Heel, M., and Patwardhan, A. (2000) Single-particle electron cryo-microscopy: towards atomic resolution. *Q. Rev. Biophys. 33*, 307−369.
28. Black, C. B., Haung H.-W., and Cowan, J. A. (1994) Biological coordination chemistry of magnesium, sodium and potassium ions. Protein and nucleotide binding sites. *Coord. Chem. Rev. 135*/*136*, 165−202.
29. Crowther, R. A., and Amos, L. A. (1971) Harmonic analysis of electron microscope images with rotational symmetry. *J. Mol. Biol. 60*, 123−130.

BI034082Q